A Single-Beam, Ponderomotive-Optical Trap for Energetic Free Electrons

Traditionally, there have been many advantages to using laser beams with Gaussian spatial profiles in the study of high-field atomic physics. High peak intensities are achieved due to their focusability, they are easily generated in most laser systems, and their focal region can be described analytically. However, free electrons interacting with such a field are rapidly accelerated out of the high-intensity region via the ponderomotive force (which is proportional to the gradient of the laser intensity).[1,2] As a result, the electrons' interaction time with the intense portions of the laser focus can be much shorter than the pulse duration. In order to observe harmonic generation from oscillating free electrons, one must first control the expulsion of electrons from the focal region.[3] This confinement can be most easily achieved by creating an intensity minimum at the focus, thereby using the ponderomotive force to push the electrons toward the central minimum. If this intensity minimum is non-zero, then the electrons can interact with intense fields while remaining trapped. Such ponderomotive trapping has been proposed in the past,[4,5] and specific laser-based schemes to trap electrons in the radial direction have been described.[6,7] To our knowledge, such focal spots have not been generated with a high-power laser. In addition, these proposed traps would not confine electrons in the axial (laser propagation) direction. In this article we will present a novel scheme to trap electrons in three dimensions with a single laser beam.

Numerical Results

A "trapping" focal region consists of an intensity minimum surrounded on all sides by higher intensities. To understand how to create such a region, it is important to adopt a formalism to describe the propagation of light. Huygens' principle, which states that we can consider every point on a wave front to be a point source for a spherical wave, makes it possible to find the field distribution in some "observation" plane if the field distribution in an earlier "source" plane is known.[8] A computer program has been written to calculate the three-dimensional focal region from an arbitrary, monochromatic laser beam. The "source" plane is the field distribution at the lens, and the "observation" plane is scanned through the focal region. The incident intensity distribution can be created mathematically (Gaussian, super-Gaussian, flat-top, etc.) or can be entered as a digitized image. The incident phase front is assumed to be uniform, and the lens is assumed to be perfect (although the addition of aberrations is possible). The beam can be passed through phase and amplitude masks on-line in an effort to alter the shape of the focal region.

By passing the beam through amplitude masks, losses are introduced into the system, yet the shape of the focal region is changed only slightly. Figure 70.13(a) shows an incident Gaussian beam [where w is the $1/e^2$ (intensity) radius]. Figure 70.13(b) shows the intensity distribution of the focal region as a function of z (axial or laser propagation direction) and r (radial direction). The Rayleigh range (z_0) and the $1/e^2$ waist (w_0) are shown in the figure. Figure 70.13(c) shows the focal spot at $z = 0$. Blocking the center of the beam [Figs. 70.13(d)–70.13(f)] or blocking an annular section [Figs. 70.13(g)–70.13(i)] has little effect on the intensity distribution near the focus. A centrally peaked distribution is formed in all cases.[9]

As Casperson has shown,[10] modulating the phase of the incident beam can result in deep far-field amplitude modulation with little loss in total energy. This can be accomplished by placing phase masks in the path of the beam. Of particular interest is the effect of binary phase plates, which add either zero or π phase to portions of the beam. If half of the Huygens' spherical waves encounter a π-phase shift while the other half do not, we can expect complete destructive interference where they meet. For a focused laser beam, this occurs at the center of the focal region. A simple, two-zoned binary phase plate is shown in Fig. 70.14(a). By passing a Gaussian beam through this plate and focusing it, an altered intensity distribution [Fig. 70.14(b)] is formed. It is important to note that this distribution is not symmetric about the z axis and, therefore, would confine particles in only one dimension. The focal spot is shown in Fig. 70.14(c). A beam similar to the TEM_{01}^{*} mode (commonly referred to as a "donut" mode) can be generated by passing a Gaussian TEM_{00} through a smoothly varying helical phase plate [Fig. 70.14(d)]. Such a phase plate has been generated for millimeter[11] as well as optical wavelengths.[12,13]

The resulting focal region [Figs. 70.14(e) and 70.14(f)] confines electrons in the radial direction only. It is also difficult to "tune" the trap minimum away from zero. A scheme has been proposed that combines a donut beam focus with a centrally peaked focus.[6] The added complexity of mixing two beams results in a focal region with a tunable center intensity, but the trap would not confine particles in the axial direction.

The binary phase plate shown in Fig. 70.14(g) contains only two zones, yet the focal spot [Fig. 70.14(i)] is surprisingly similar to the one generated by the complicated helical plate. The donut shape near $z = 0$ confines electrons in the radial direction, and the centrally peaked regions away from $z = 0$ provide axial trapping [see Fig. 70.14(h)]. The focal region is shown in detail in Fig. 70.15. The π region of the phase plate

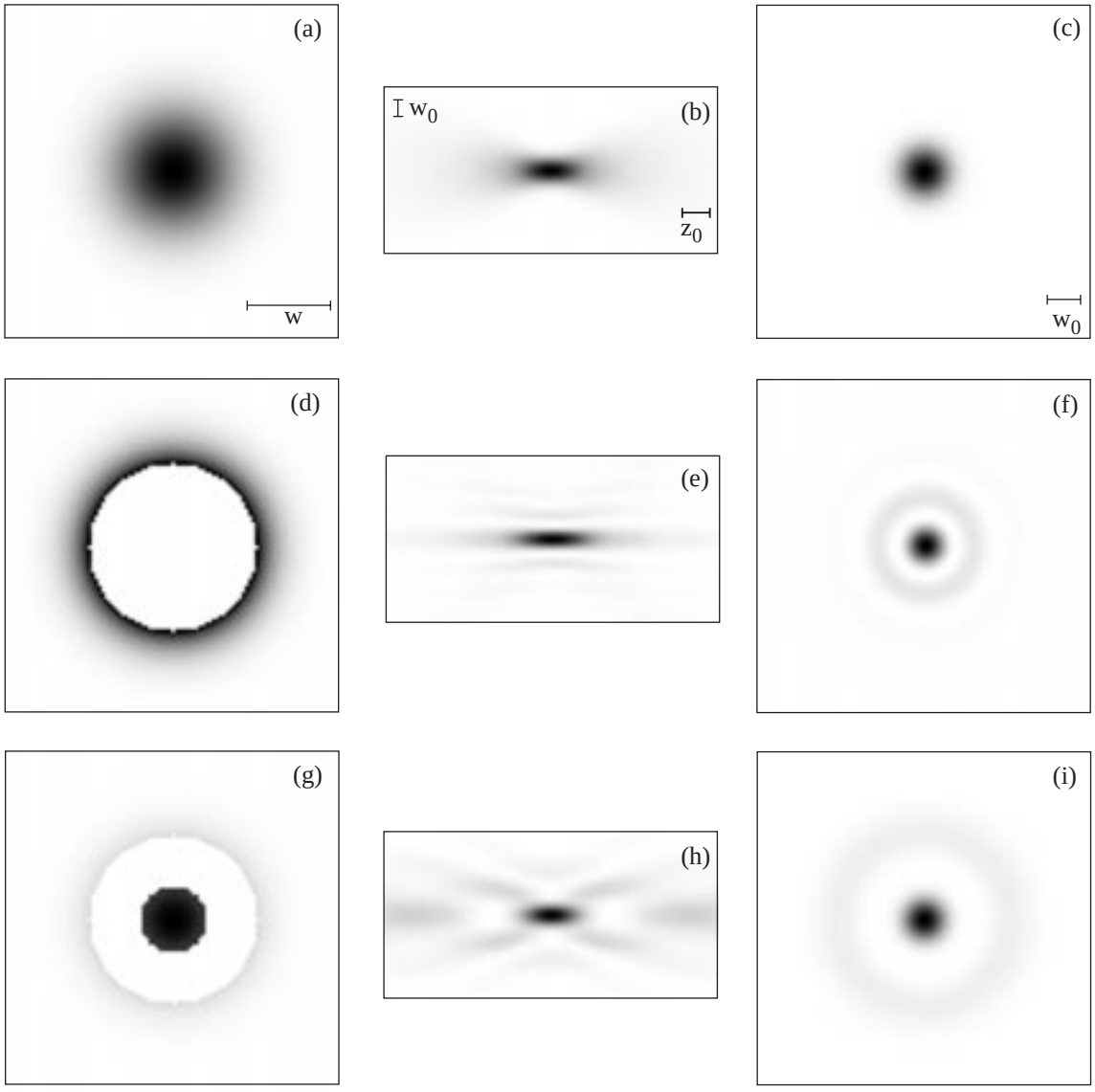

Figure 70.13
The effects of amplitude masking on the intensity distributions of a focused Gaussian beam. The first column shows three different near-field intensity distributions. The second column shows the intensity distributions as a function of z and r (the center of each image corresponds to $z = 0$, $r = 0$). The third column shows the focal spots. In order to show the maximum contrast, each image is normalized to its peak value. Note that all of the focal regions are centrally peaked.

has a diameter of 1.65 w [where w is the $1/e^2$ (intensity) radius of the incident Gaussian beam]. This results in a π-phase shift for half of the incident field. The calculated intensity in the focus is normalized to the peak intensity in the absence of the phase plate. The r and z positions are normalized to the unaltered beam waist w_0 ($1/e^2$ radius) and the unaltered beam Rayleigh range z_0, respectively. Figure 70.15(a) shows a surface plot and Fig. 70.15(b) shows a contour plot of the trapping region. There is an exact zero in intensity at the center of the focus, with intensity walls ranging from ~8% to ~30% (of the unaltered peak intensity) in all directions. The trapping region has a volume of complete trapping of $\sim 2w_0^2 z_0$ (bound by the solid contour line of 8.2%). By changing the size of the π region of the phase plate (or, equivalently, by changing the size of the incident beam), the destructive interference at the center of the focus will not be complete, creating a non-zero minimum. Figure 70.16(a) shows the calculated focal distribution for a Gaussian beam incident on a phase plate with a

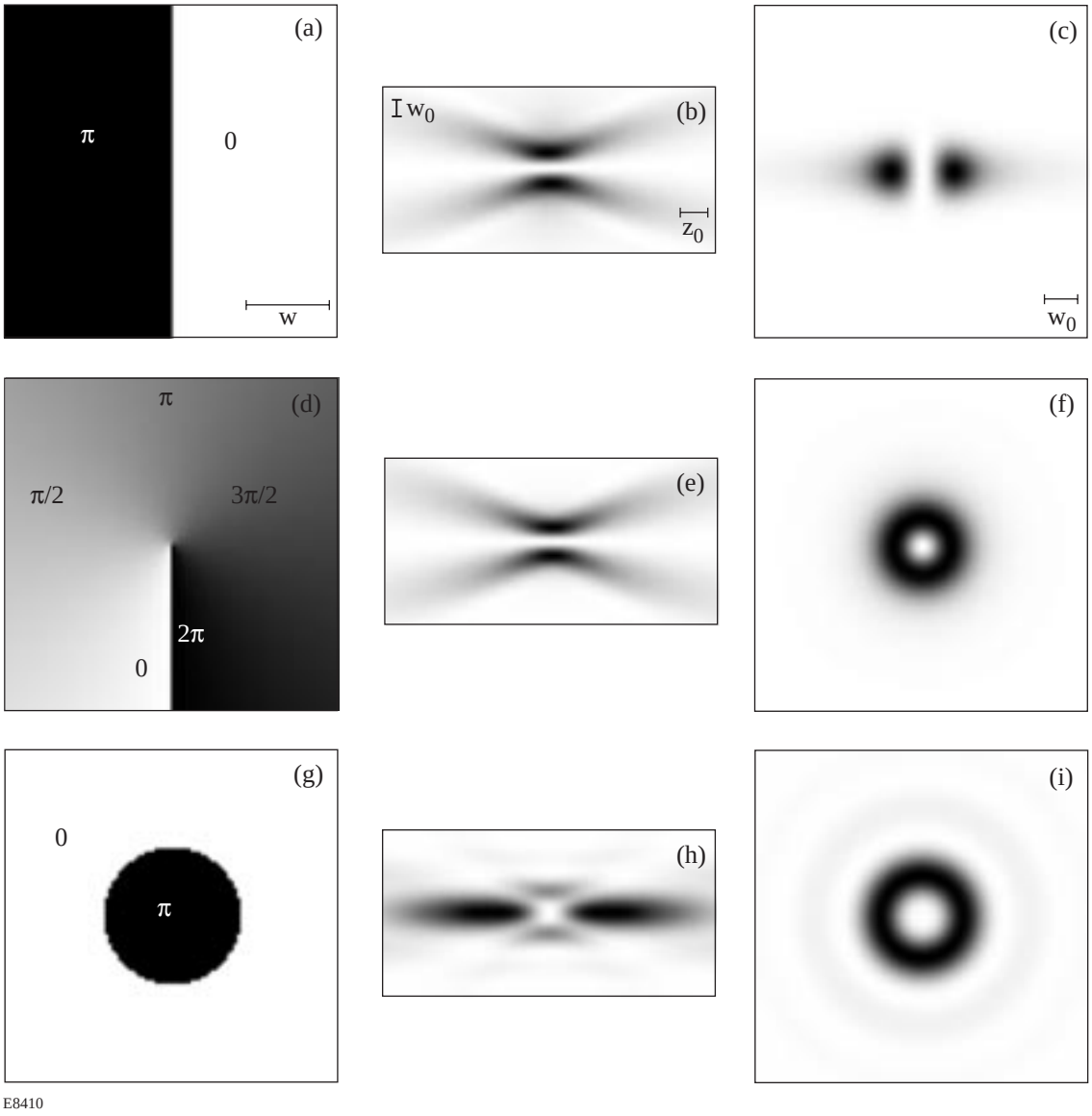

Figure 70.14
The effects of phase masking on the intensity distributions of a focused Gaussian beam. The first column shows three different phase masks. The second column shows the intensity distributions as a function of z and r (the center of each image corresponds to $z = 0$, $r = 0$) when the phase mask is placed before the incident beam. The third column shows the focal spots. In order to show the maximum contrast, each image is normalized to its peak value.

π-region diameter of 2.20 w. Figure 70.16(b) shows a contour plot of the trapping region. In this case, the bottom of the trap is ~17% of the unaltered beam peak intensity, and the trap walls range from ~24% to ~50%. The trapping volume is $\sim w_0^2 z_0$. This focal region is ideal for trapping electrons in a high-field region.

Experimental Setup

The phase masks described above can be made by using photolithographic techniques. However, for the particularly simple geometry that produces a suitable trapping region, a novel segmented wave-plate approach has been developed. A half-wave plate is typically used to rotate the polarization angle of an incident, linearly polarized beam of light. This is a result of the retardation of π phase between two orthogonal incident polarizations. However, if part of the incident beam can be made to travel through the plate as a fast wave while the other travels as a slow wave, a π-phase shift will be created between the two portions. To accomplish this, a 4-cm disk was cut from the center of an 8-cm mica half-wave plate. The disk and annulus were then mounted individually on cross hairs and aligned to the beam path (as shown in Fig. 70.17). In Fig. 70.17, the laser is polarized in the vertical direction, and the annulus is arranged such that its *e* axis is vertical, while the disk has its *o* axis vertical. This results in a π-phase shift of a portion of the incident field. The size of the disk was chosen such that approximately half of the incident field passed through it. This resulted in near-zero intensity at the center of the focus. By rotating the two pieces as a unit, one can rotate the polarization of the incident beam without introducing additional optics or changing the shape of the focal region. Also, as long as one does not require a single polarization direction in the focal

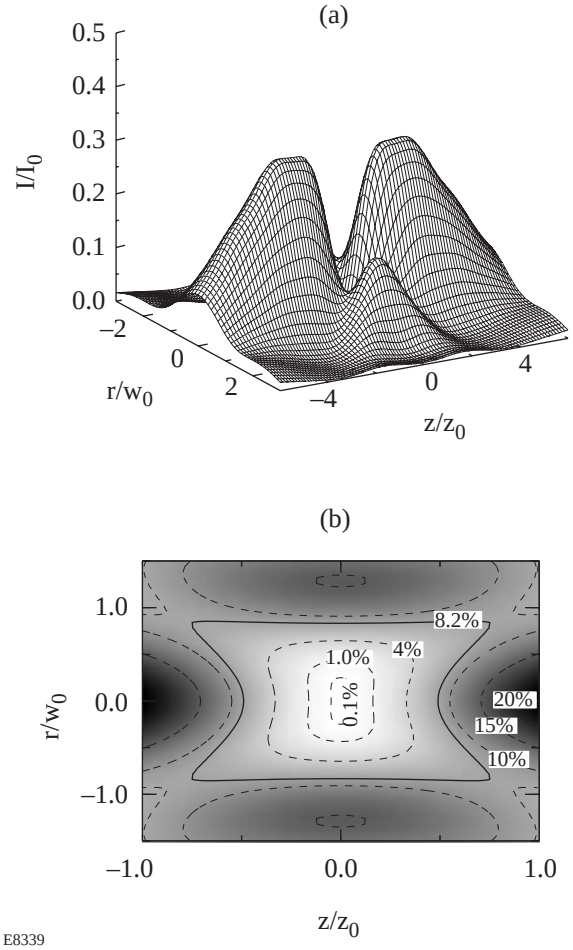

Figure 70.15
(a) A computer-generated trapping focal region with zero intensity at its center (π-region diameter = 1.65 w). (b) A contour plot of the trapping region. The volume of complete trapping is bound by the solid contour line at 8.2%.

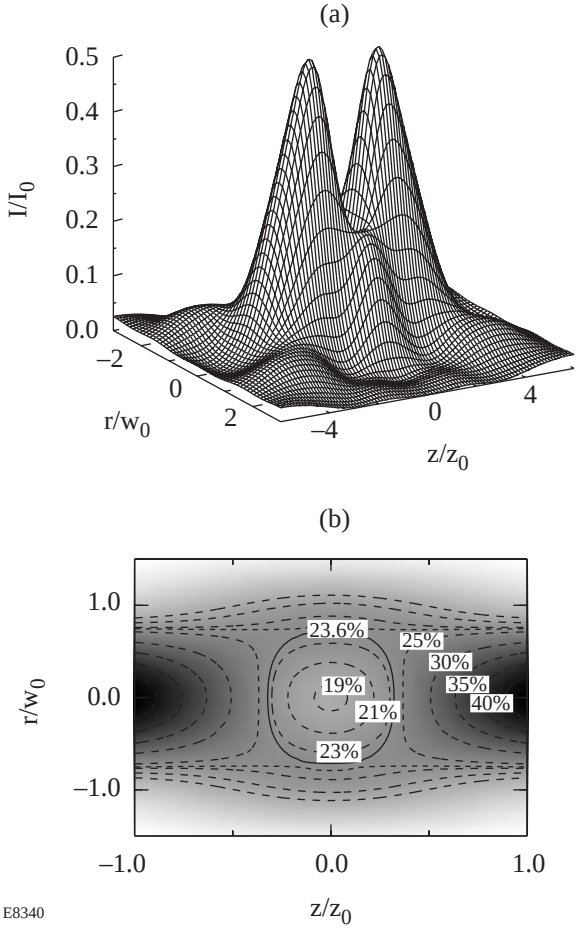

Figure 70.16
(a) A computer-generated trapping focal region with 17% intensity at its center (π-region diameter = 2.20 w). (b) A contour plot of the trapping region. The volume of complete trapping is bound by the solid contour line at 23.6%.

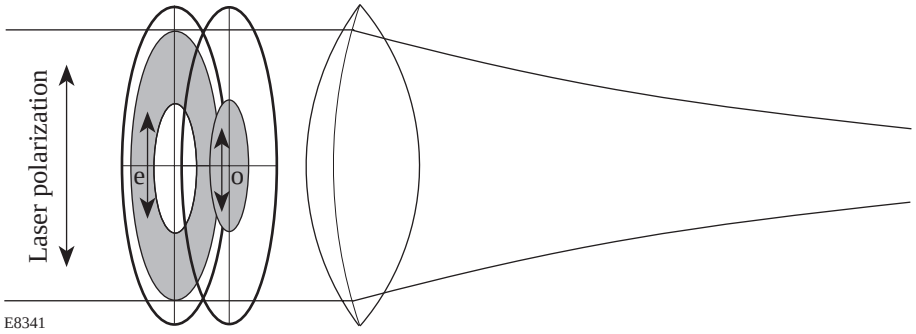

Figure 70.17
The experimental setup for the segmented wave-plate technique for generating a trapping focal region.

region, the depth of the trap can be tuned by rotating the central disk away from 90°. This results in a polarization rotation of the inner portion of the beam, which will put some of the field into the noninterfering orthogonal polarization, thereby filling in the minimum. The extreme case is to rotate the disk a full 90°, back to its original position, which produced an ordinary, centrally peaked focus.

Experimental Results

To image the altered focal spot, the wave-plate arrangement was aligned to the beam path of the tabletop terawatt laser (T^3) directly before the focusing lens (f = 212 cm).[14] The focal region was imaged with a CCD camera coupled to a 10× microscope objective (Fig. 70.18). The camera-objective combination was moved together to map out the focal region. A single laser shot was taken at each position, and each image was minimally smoothed and background subtracted. The scan was generated with ~40-mJ, ~2-ps infrared laser pulses. By firing the final, single-pass amplifier, energies of ~1 J are achieved with no noticeable change in the near- or far-field characteristics of the beam. The unaltered beam's peak intensity typically reaches 10^{18} W/cm^2.

Figure 70.19(a) shows the focal spot created without the wave-plate arrangement in place. The beam diameter is approximately 1.5× the diffraction limit. Figure 70.19(b) shows the focal spot with the wave-plate arrangement set to 90°. Despite the deviation of the unaltered beam from the diffraction limit, there is a well-defined minimum in the center of the altered spot. Figure 70.19(c) shows the focal spot with the wave-plate arrangement in place, but set to 0°. Here, the wave plate is set to its original, unaltered configuration, and the beam has returned to its original shape. Figures 70.20(a) and 70.20(b) show the lineouts of the altered beam in the x and y directions at $z = 0$. The x and y positions are normalized to the experimentally determined beam waist of the unaltered beam. Figure 70.20(c) shows the intensity of the beam at $r = 0$ as a function of z. The intensities in Fig. 70.20 are normalized to the peak intensity of the unaltered beam.

A more detailed scan was made with a continuous-wave beam (the oscillator of the T^3 laser). Figure 70.21 shows two slices through the focal volume along the z axis. Figure 70.21(a) shows the intensity distribution in the plane $y = 0$, and Fig. 70.21(b) shows the distribution for $x = 0$. In each

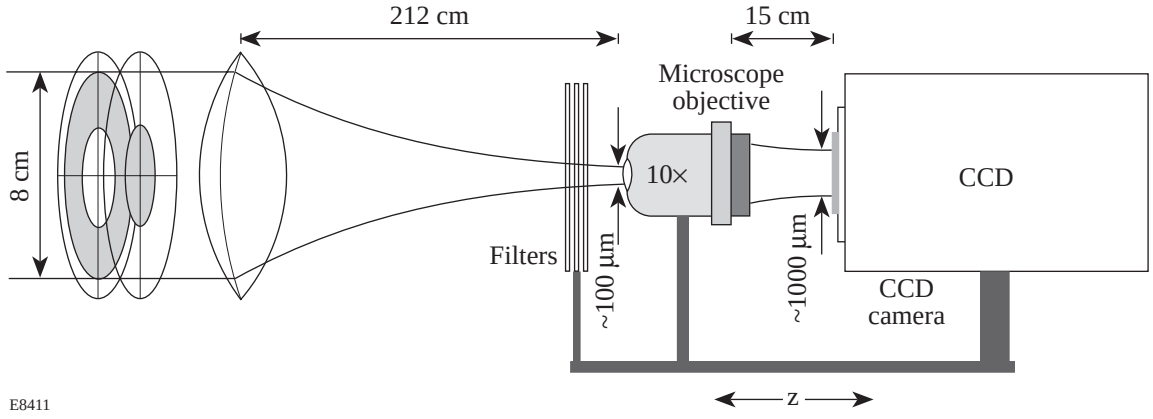

Figure 70.18
The experimental setup for imaging the altered focal region. Here $z = 0$; i.e., the object plane of the microscope objective coincides with the focal plane of the lens.

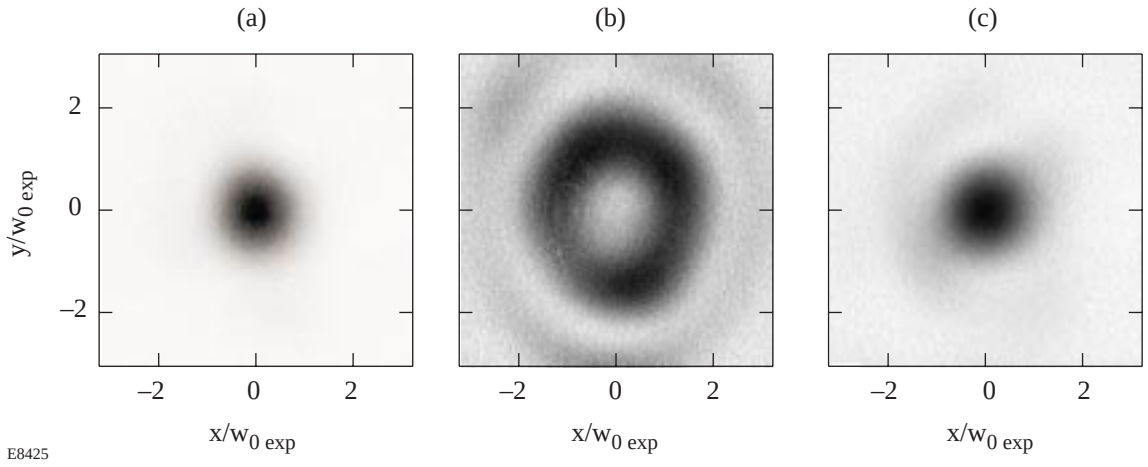

Figure 70.19
Focal spots (a) without the wave-plate arrangement in place, (b) wave-plate setup in place and set to 90°, and (c) wave-plate setup in place and set to 0°.

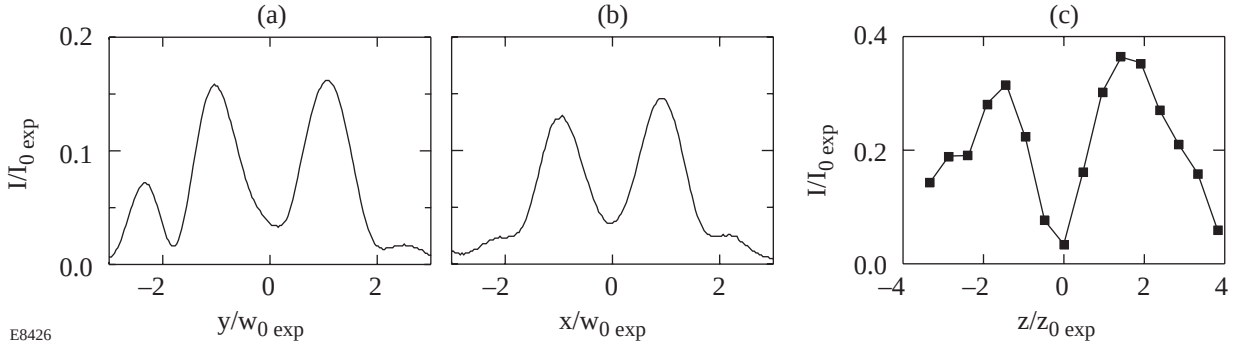

Figure 70.20
Lineouts of the trapping focal region. (a) Lineout in the x direction, (b) lineout in the y direction, and (c) the intensity at $r = 0$ as a function of z. All axes are normalized to the experimentally determined values for the unaltered beam (spot size for the x and y positions, Rayleigh range for the z positions, and unaltered beam peak intensity for the intensity values).

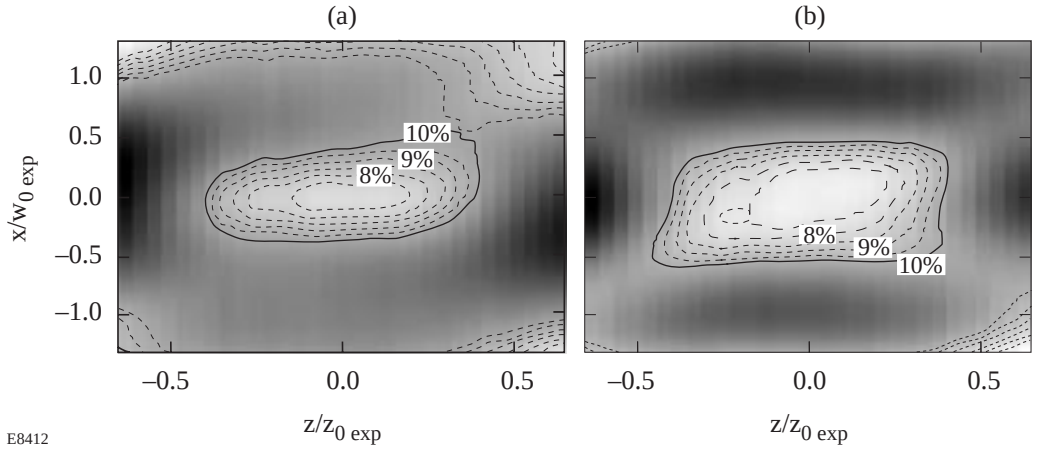

Figure 70.21
Contour plots of the trapping focal region. (a) In the plane $y = 0$ and (b) in the plane $x = 0$. The experimentally observed volume of complete trapping is bound by the solid contour line at 10%.

plot, there is a region of complete trapping bound by intensity walls of 10% (solid line) of the unaltered beam's peak intensity. Although the incident beam size was not matched with the size of the wave-plate pieces, a sufficiently large portion of the incident field was shifted to create a trapping region. These experimentally obtained distributions (using a pulsed or cw beam) exhibit a local minimum in intensity at the *origin along all three dimensions*, making them suitable focal regions for ponderomotive trapping.

Summary

In summary, we have produced, for the first time to our knowledge, a tunable, single-beam, three-dimensional, ponderomotive-optical trap for free electrons with a high-peak-power laser system. Neutral atoms and macroscopic, low-index particles could also be trapped in the low-field region. We have presented a novel, segmented-wave-plate approach as an alternative to a phase mask, along with experimental confirmation of the intensity distribution of the altered focal region. Experiments to image the linearly and nonlinearly scattered light (both 1ω and 2ω) from the trapped electrons are being carried out.

ACKNOWLEDGMENT

The author wishes to thank A. Maltsev for machining the half-wave plate. This study is supported by the National Science Foundation with additional support from the U.S. Department of Energy Office of Inertial Confinement Fusion under Cooperative Agreement No. DE-FC03-92SF19460, the University of Rochester, and the New York State Energy Research and Development Authority. The support of DOE does not constitute an endorsement by DOE of the views expressed in this article.

Appendix A: Huygens' Principle

Huygens' principle states that we can consider every point on a wavefront to be a point source for a spherical wave.[8] As a result, if one knows the field in some "source plane (S')," it is then possible to add the contributions from the individual spherical waves to find the field distribution in an "observation plane (S)" (see Fig. 70.22). The spherical wave emanating from a tiny element of area $\Delta a'$, surrounding the point $(x',y',0)$ in the source plane, results in a contribution to the field in the observation plane,

$$\Delta\varepsilon(x,y,z) = -(i/\lambda)\left(e^{ikr}/r\right)\,\varepsilon(x',y',0)\,\Delta a', \qquad \text{(A1)}$$

where

$$r = \left[(x-x')^2 + (y-y')^2 + z^2\right]^{1/2}, \qquad \text{(A2)}$$

$k = 2\pi/\lambda$, $\Delta a' = dx'dy'$, and $\varepsilon(x',y',0)$ is the electric field (magnitude and phase) in the source plane. For most applications, we may make the Fresnel approximation

$$z^3 >> (\pi/4\lambda)\left[(x-x')^2 + (y-y')^2\right]^2_{\max} \qquad \text{(A3)}$$

and sum up all of the field contributions with the integral

$$\varepsilon(x,y,z) \approx -\left(ie^{ikz}/\lambda z\right)\iint \varepsilon(x',y',0)\,\exp\left\{ik\left[(x-x')^2 + (y-y')^2\right]/2z\right\}dx'dy'. \qquad \text{(A4)}$$

To calculate the field at the point (x,y,z), $\varepsilon(x',y',0)$ must be known for all (x',y'). Equation (A4) can then be solved numerically.

For the case of a laser beam incident on a positive lens, the intensity distribution can be assumed to be Gaussian (as is typical for many laser systems) or it can be determined experimentally by imaging the near-field distribution. Determining the phase of the incident field is more complicated, as it involves interferometric methods.[15] If the laser is well collimated and is found to focus to a spot size close to the diffraction limit, then the phase front can be assumed to be uniform. The effect of the lens is to simply add a phase proportional to the thickness of the lens material at any point. A plano-convex lens results in a "spherical" phase distribution,

$$\Phi(r') = k\left(f^2 - r'^2\right)^{1/2} \qquad \text{(A5)}$$

where f is the focal length of the lens and $r'^2 = x'^2 + y'^2$ is the square of the radial location in the source plane. If we assume that $f^2 >> r'^2$ (the paraxial approximation), then we can perform a binomial expansion,

$$\Phi(r') = kf\left(1 - r'^2/2f^2 - r'^4/8f^4 - \ldots\right). \qquad \text{(A6)}$$

The first term adds a constant phase to the entire beam and can be discarded, as can the higher-order terms since they are vanishingly small. By keeping only the quadratic term, we are left with a "perfect" lens in the context of this approach (in practice, aspherical lenses are not purely parabolic). A Gaussian laser beam that has passed through this lens will have the field distribution

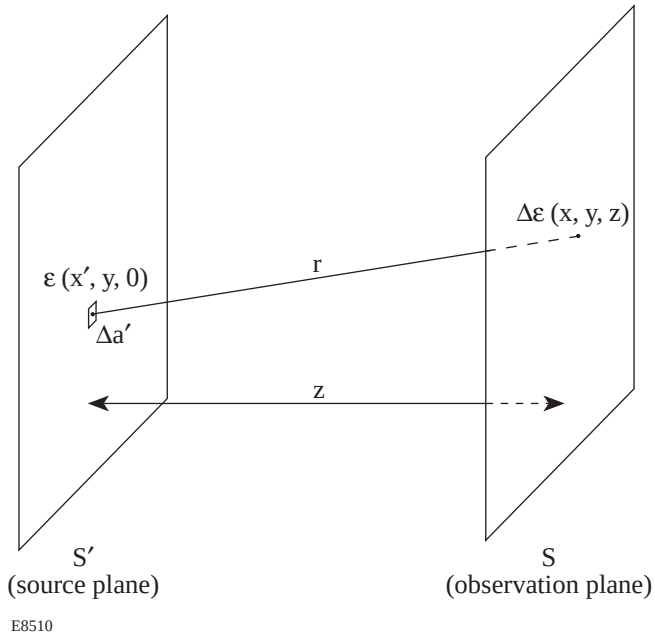

Figure 70.22
The geometry of the Huygens' wave approach to the propagation of light. The source and observation planes are separated by a distance *z*. The locations in the source plane are denoted with a prime (′), while the locations in the observation plane are left unprimed.

$$\varepsilon(x', y', 0) = A \exp\left(-r'^2/w^2 - ikr'^2/2f\right), \qquad \text{(A7)}$$

where A is the field amplitude and w is the beam radius at the $1/e$ point in the electric field amplitude (which is equivalent to the $1/e^2$ point in intensity). It should be pointed out that all calculations in both this article and the computer codes use the scalar-wave approach.

REFERENCES

1. H. A. H. Boot and R. B. R.-S.-Harvie, Nature **180**, 1187 (1957).
2. C. I. Moore, J. P. Knauer, and D. D. Meyerhofer, Phys. Rev. Lett. **74**, 2439 (1995).
3. E. S. Sarachik and G. T. Schappert, Phys. Rev. D **1**, 2738 (1970).
4. V. Gaponov and M. A. Miller, J. Exptl. Theoret. Phys. (U.S.S.R.) **34**, 242 (1958).
5. N. J. Phillips and J. J. Sanderson, Phys. Lett. **21**, 533 (1966).
6. C. I. Moore, J. Mod. Opt. **39**, 2171 (1992).
7. U. Mohideen *et al.*, J. Opt. Soc. Am. B **9**, 2190 (1992).
8. P. W. Milonni and J. H. Eberly, *Lasers* (Wiley, New York, 1988).
9. J. Peatross, J. L. Chaloupka, and D. D. Meyerhofer, Opt. Lett. **19**, 942 (1994).
10. L. W. Casperson, Opt. Quantum Electron. **10**, 483 (1978).
11. G. A. Turnbull *et al.*, Opt. Commun. **127**, 183 (1996).
12. M. W. Beijersbergen *et al.*, Opt. Commun. **112**, 321 (1994).
13. K. T. Gahagan and G. A. Swartzlander, Jr., Opt. Lett. **21**, 827 (1996).
14. Y.-H. Chuang, D. D. Meyerhofer, S. Augst, H. Chen, J. Peatross, and S. Uchida, J. Opt. Soc. Am. B **8**, 1226 (1991).
15. Laboratory for Laser Energetics LLE Review **31**, NTIS document No. DOE/DP/40200-47, 1987 (unpublished), p. 114.